Optics Letters

# Real-time capture of single particles in controlled flow by a rapidly generated foci array with adjustable intensity and pattern

Chenchu Zhang,[1] Ye Hanchang,[1] Chaowei Wang,[2,*] Jingjing Zhang,[3] Linhan Zhao,[1] Heng Zhang,[1] Wulin Zhu,[2] Hua Zhai,[1] Wu Dong,[2,5] and Koji Sugioka[4]

[1]Anhui Province Key Lab of Aerospace Structural Parts Forming Technology and Equipment, Institute of Industry and Equipment Technology, Hefei University of Technology, Hefei 230009, China
[2]Hefei National Laboratory for Physical Sciences at the Microscale and CAS Key Laboratory of Mechanical Behavior and Design of Materials, Department of Precision Machinery and Precision Instrumentation, University of Science and Technology of China, Hefei 230026, China
[3]School of Mathematical Sciences, Anhui University, Hefei 230601, China
[4]RIKEN Center for Advanced Photonics, 2-1 Hirosawa, Wako, Saitama 351-0198, Japan
[5]e-mail: dongwu@ustc.edu.cn
*Corresponding author: chaoweiw@ustc.edu.cn

Received 13 August 2021; revised 28 September 2021; accepted 29 September 2021; posted 29 September 2021 (Doc. ID 440494); published 19 October 2021

**We propose a new, to the best of our knowledge, technique to capture single particles in real-time in a microfluidic system with controlled flow using micro-pillar traps fabricated by one-step. The micro pillars are fabricated in parallel by femtosecond multi-foci laser beams, which are generated by multiplexing gratings. As the generation process does not need integration loops, the pattern and the intensity distribution of the foci array can be controlled in real-time by changing the parameters of gratings. The real-time control of the foci array enables rapidly fabricating microtraps in the microchannel with adjustment of the pillar spaces and patterns according to the sizes and shapes of target particles. This technology provides an important step towards using platforms based on single-particle analysis, and it paves the way for the development of innovative microfluidic devices for single-cell analysis.** © 2021 Optical Society of America

https://doi.org/10.1364/OL.440494

In recent years, single-cell analysis has played a key role in molecular diagnosis [1], medical treatment [2], cell biology [3], and some other fields [4–6]. Microtrapping technology, which is used to hold cells/particles for further analysis [7–9], provides an important platform for biomedical and biochemical research. Among microtrap technologies, microtrapping based on microfluidic chips is particularly outstanding because of its low cost, less reagent consumption, and simple cell operation [10–12]. Various methods have been proposed to capture a large number of suspended particles by integrating the traps in microfluidic chips. For example, acoustic traps [13], micropores [14], dielectric electrophoresis [15], and hydrodynamic traps [16,17] have been utilized to capture microparticles to form arrays of microparticles or cells.

Compared with the above methods, the hydrodynamic array trapping method has the advantage of simple operation, which is the most commonly used method in microfluidic systems. In the microfluidic channel, microtrap arrays corresponding to the size of the target particles are manufactured in advance, and then the particles or cells mixed in liquid are injected into the microfluidic chip and captured by the trap array. However, constant external pressure is needed to keep the particles or cells trapped. Moreover, as the hydraulic resistance of the microchannel is smaller than that of the trap array, most particles will bypass the traps, which results in a relatively low capture efficiency (10%). To solve this problem, a real-time two-photon lithography in control flow was proposed, which greatly improved the capture efficiency based on the one-bead-to-one trap approach [18].

In the real-time capture approach, the key factor is the capture time, which greatly influences the total operating time. Applying the foci array of laser beams to create multi-traps in parallel in a single exposure instead of in a single focus exposure will save the capture time by a factor of several times. The foci array can be generated by conventional approaches such as Dammann grating [19], microlens array [20], and computer-generated hologram (CGH) [21]. However, the Dammann grating and the microlens array do not allow for freely adjusting the intensity uniformity of the foci, which makes it impossible to compensate for the errors in the optical setup. Meanwhile, the CGH requires iteration loops, which will also not be suitable for real-time adjustment. Herein, we present a rapid generation method of the foci array with adjustable intensity distribution and without iteration loops. Based on this approach, a real-time microfluidic trapping (RT-MFT) method has been put forward to rapidly capture single particles for further analysis. First, the multi-foci array with adjustable intensity distribution is generated by multiplexed gratings. The intensity distribution can be controlled by multiplexing a two-dimensional (2D) Dammann

grating with a blazed grating, which is more efficient than integration methods such as the weighted Gerchberg–Saxton (GS) algorithm [22]. Furthermore, the patterns and gap sizes of the foci array can be easily adjusted by changing the parameters of gratings depending on the requirements for trapping target particles. Then, the real-time generated foci array can capture the particles in a very short time (100 ms), which is several times, or even dozens of times, faster than that of the traditional hydrodynamic trap. Importantly, after capturing the target particle, there is no need to supply continuous external pressure, which improves the simplicity of the system. To demonstrate the RT-MFT as an effective method for single-particle capture and analysis and then to provide the fabricated system as a planform for biomedical and biochemical research, the fabrication parameters of traps are studied and optimized.

A multi-foci array was generated by using multiplexed gratings. Several 2D Dammann gratings were set at certain angles to separate the beams into various directions. The foci array forms a square pattern when the angle is set at 90° and a hexagon pattern at 60°, as shown in Figs. 1(a) and 1(b). The spacing of the foci can be adjusted by changing the period of 2D Dammann gratings, by which pillar arrays with different spacing can be created, as shown in Figs. 1(c) and 1(d). The intensity uniformity of each focus in the array is almost 100% if the incident beam has an ideal Gaussian profile to generate the concentric pattern with the hologram. However, it is difficult to experimentally create the ideal Gaussian beam. Therefore, the uniformity of the hologram needs to be optimized according to the actual profile of the laser beam used. To solve this problem, we propose an approach that combines the multiplexing of Dammann gratings with blazed gratings. The intensity distribution of the foci array can be controlled by the modulation phase depth of the blazed grating, which is rapid and straightforward so as not to require an iterative process.

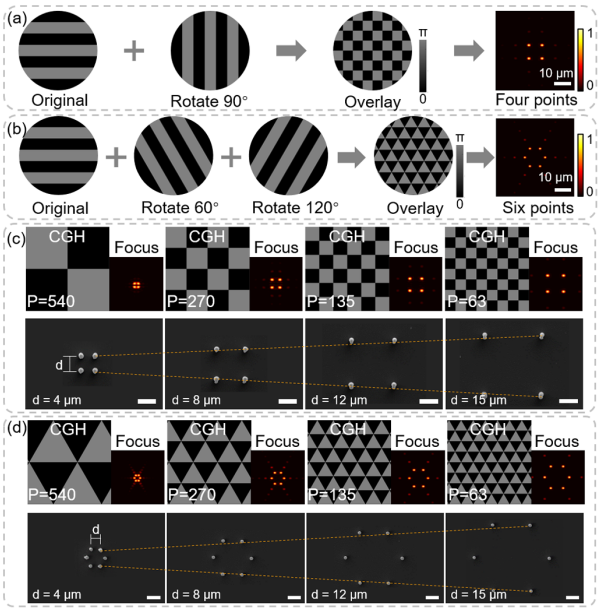


**Fig. 1.** Multiplexing procedure of grating to generate pattern-controllable foci-array. The array pattern becomes square (a) when the angle of the Dammann gratings is set at 90° and hexagon (b) at 60°. (c) and (d) show that the spacing of the foci can be adjusted by changing the period of the Dammann gratings with the scanning electron microscope images (lower) of the pillars array with different spacing created by the corresponding period of Dammann gratings (upper). The P in (c) and (d) is the period of corresponding grating (pixels).

The principle of multi-foci generation by combining the multiplexed 2D Dammann gratings and the blazed gratings is simple. For example, to generate four foci, two points with a uniform distribution are created by the 2D Dammann grating first. Then, the blazed grating with adjustable modulation phase depth is added onto the Dammann grating. Finally, the intensity distribution between the 0 order and the 1st order of the blazed grating can be adjusted by the phase depth of blazed grating, as shown in Fig. 2(a). The diffraction efficiency of grating can be given as follows:

$$\eta = \left[\sin c\left(\frac{n}{2}\right) \times \cos\left(\frac{n\pi}{2} + \frac{\varphi}{2}\right)\right]^2, \quad n = 0, \pm 1, \pm 2, \pm 3. \tag{1}$$

Here, $n$ is the diffraction order, and $\varphi$ is the modulation depth of grating. The diffraction efficiency is influenced by the modulation depth $\varphi$. Figure 2(b) shows the relationship between the intensity distribution of the 0 order and the 1st order and the modulation depth $\varphi$. In Fig. 2(c), $\varphi$ is set at $0.6\pi$, resulting in the intensity of the 0 order being about 3 times larger than that of the 1st order. The more intuitive relationship between the 1st order (top points) and the 0 order (bottom points) is tested in the experiment, as shown in Fig. 2(d). In the experimental condition, the average point was found to be slightly deeper than $\pi$, which was probably caused by some small deviations in the optical setup, such that the peak of the Gaussian beam did not exactly illuminate the center of spatial light modulator (SLM, Holoeye Pluto NIR-II), or the beam axis might have a slight misalignment to the vertical axis of the photoresist surface.

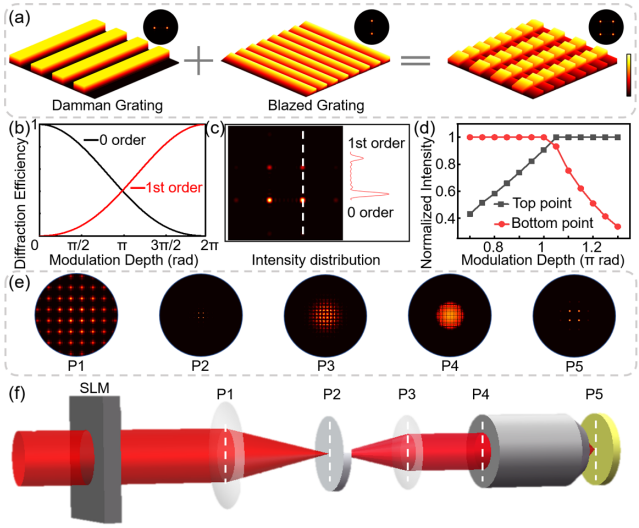


**Fig. 2.** (a) Intensity distribution can be controlled by the multiplexed Dammann gratings combined with the blazed gratings. (b) Relationship between the diffraction efficiency of the 0 order and the 1st order and the modulation depth of blazed grating. (c) 2D distribution of four foci when $\varphi$ is $0.6\pi$ (left), and the intensity profile along the dotted line in the left figure (right). (d) Experimentally tested relationship between the 1st order (top points) and the 0 order (bottom points) intensities and the modulation phase depth of the blazed gratings. (e) Simulated intensity distribution at different points along the optical path. (f) Schematic diagram of the optical system generating the multi-foci.

To further optimize the parameters of gratings for fabrication of microtraps, the intensity distribution along the optical path was simulated by the full-path optical calculation method [23], as shown Figs. 2(e) and 2(f). The intensities at P1, P2, P3, and P4 were calculated by the scalar diffraction approach. Meanwhile, the intensity at P5 was calculated by the vector diffraction approach, as the numeral aperture of objective lens was 0.8. It is worth noting that the light field is cut at P4, the entrance pupil of the objective, which influences the whole intensity at P5. When applying a grating with a smaller period, more intensity will be cut at P4, making the intensity of P5 lower than that of the larger period.

The fabrication step of the microchannel for the RT-MFT is schematically illustrated in Fig. 3(a). The fabrication of the microchannel was carried out using a conventional polydimethylsiloxane (PDMS)–glass substrate prepared by a soft lithography method. The formed channel is 25 μm wide, 25 μm high, and 8 mm long. Finally, the exfoliated film was adhered to the glass substrate to seal the microchannel.

The RT-MFT approach is a real-time capture method that takes advantage of the femtosecond laser two-photon lithography in the microchannel, as shown in Fig. 3(b). The microchannel was connected with a single inlet and a single outlet for easy operation. Silica particles with a diameter of 20 μm were mixed with liquid photo-curable resin IPL, which was then injected into the microchannel from the inlet. In the capture process, the flow stops for 550 ms to settle down the particles. Then, multi-foci generated by using the SLM was irradiated around the target particle to form a trapping array. In order to capture a single target particle immediately, the femtosecond laser focused with a 50× objective lens (NA = 0.8) scanned from the surface of the glass to the top of the PDMS channel with a scanning step of 2.4 μm and a speed of 50 μm/s.

The four-pillar trap structure can be manufactured in less than 100 ms. Figure 3(c) shows the optical microscopy images of the real-time trapping procedure. The dynamic process of capture is shown in Visualization 1. It also confirms that the captured particle is not damaged by laser irradiation.

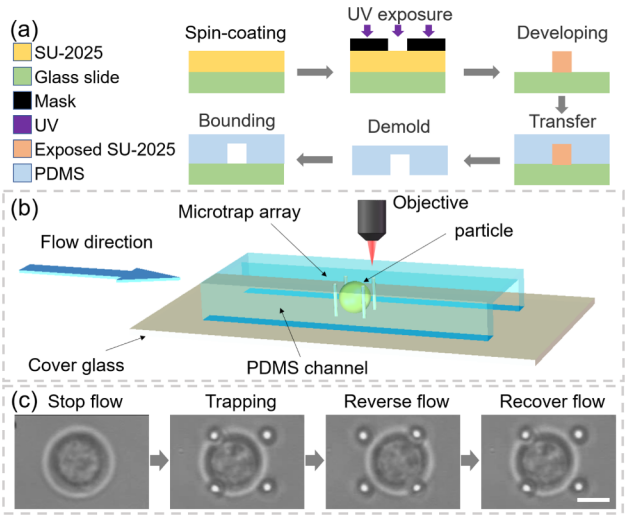


**Fig. 3.** (a) Fabrication step of microchannel for RT-MFT. (b) Schematic diagram of the RT-MFT approach by taking advantage of femtosecond laser two-photon lithography in the microchannel. (c) Optical microscopy images of the real-time trapping procedure. Scale bar is 10 μm.

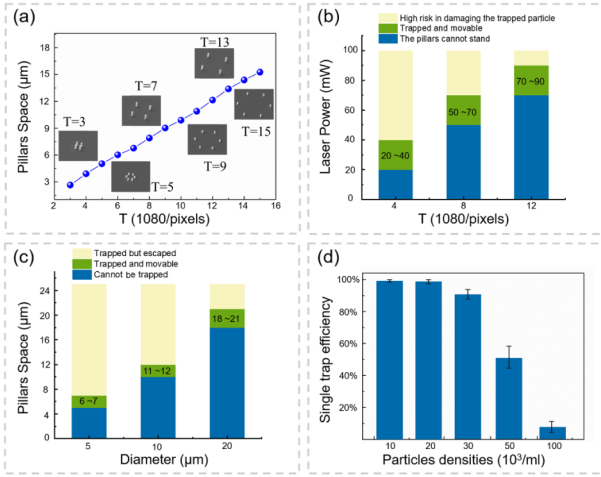


**Fig. 4.** Parameter investigations of the RT-MFT. (a) The relationship between different periods of gratings T and the pillar spaces. (b) Relationship between the laser power and the different periods of gratings T for successful trapping. (c) Relationship between the pillar space of microtraps and the size of captured particles for successful trapping. (d) Influence of the single-particle capture efficiency on the particle density.

The key experimental parameters of the RT-MFT are quantitatively investigated, as shown in Fig. 4. Figure 4(a) demonstrates the relationship between different periods of gratings and the pillar spaces, where T is defined as 1080/pixels. Trap arrays with different pillar spaces can be created by using gratings with different T. In this way, the spacing of the traps can be easily adjusted from 2.7 μm to 15.1 μm. In addition, to optimize the fabrication parameters of the microtraps, the relationship between the laser power and the different periods of gratings T for successful trapping was investigated [Fig. 4(b)]. Here, we determine appropriate standards of array traps, by which the trapped particles can slightly move inside the microtraps without sticking to the pillars. When the laser power is insufficient, the pillar cannot be supported, which results in poor stability. On the other hand, when the laser power is too high, the risk of laser damage will increase. According to the experiment results, the appropriate laser power is different for the different grating periods. The appropriate powers are examined to be 20 ∼ 40 mW, 50 ∼ 70 mW, and 70 ∼ 90 mW for T of 4, 8, and 13, respectively. The power is measured in P2 of Fig. 2(f). This phenomenon can be explained in the pull-path optical simulation, as shown in Fig. 2(e). For the gratings with higher T, the 1st order diffraction angle is higher than that of the gratings with lower periods, resulting in more energy loss in the entrance pupil of the objective lens.

Besides the relationship between the pillar space of the microtraps, the size of the captured particles for successful trapping was also investigated and can be seen in Fig. 4(c). The microtrap with the pillar space of 12 μm is suitable for non-destructive trapping of 10 μm particles. A narrower space (10 μm) may cause particles to adhere to the pillar or damage the particles, while a wider pillar space (13 μm) cannot capture the particles. The appropriate space ranges for the particles with diameters of 5 μm, 10 μm, and 20 μm are 7 μm, 12 μm, and 22 μm, respectively. Meanwhile, pure liquid resin IPL is known to be too viscous to flow smoothly, which requires additional dilution to adjust the viscosity for injection and flow operations. Finally, we studied the influence of the single-particle capture

efficiency on the particle density, as shown in Fig. 4(d). When the particle solubility is in the proper range of $0 \sim 20{,}000/\mathrm{mL}$, the single-particle capture efficiency can reach to 100%. When solubility is increased to 30,000/mL, the single- capture efficiency decreases to 90%, and the particle solubility exceeding 30,000/mL significantly decreases the single-capture efficiency. The single-capture efficiency is lower than 35% when the particle solubility increases to 100,000/mL. This is due to the increase in particle concentration that causes the particle aggregation, and individual particles cannot be separated. In most actual single-cell analysis conditions, the cell density is generally not too high, making the RT-MFT method suitable for general single-cell analysis.

In summary, we proposed a real-time generation approach of multi-foci with adjustable pattern and intensity. Based on this approach, an RT-MFT method that achieves reliable single-particle capture has been presented. This novel method offers the additional advantage of not requiring an iterative process. Thus, the RT-MFT method has several advantages that provide superior characteristics to the traditional hydrodynamic capture methods. First, the capture efficiency can attain 100%, which completely solves the problem of low capture efficiency in traditional methods. Second, since the RT-MFT method employs no predesigned array traps in the microchannels and performs real-time fabrication, it enables *in situ* fabrication of traps with flexible designs depending on the size of the target particles. Third, this method does not require continuous external pressure to maintain particle capture, which greatly improves the simplicity of the device. Finally, the target particles can be accurately captured, and the non-target particles can be released, indicating that our method does not require prefiltration, thus further enhancing the simplicity of the system. We believe that the proposed RT-MFT method is useful for single-cell analysis by applying a flow medium with better biocompatibility, such as hydrogels, and it provides a new direction for single-particle capture.

**Funding.** National Natural Science Foundation of China (11801126, 62005262, 62105090); Fundamental Research Funds for the Central Universities (PA2020GDSK0077); China Postdoctoral Science Foundation (2020M671888, 2021T140649); National Key Research and Development Program of China (2018YFB1105400).

**Disclosures.** The authors declare no conflicts of interest.

**Data Availability.** Data underlying the results presented in this paper are not publicly available at this time but may be obtained from the authors upon reasonable request.

## REFERENCES

1. D.-K. Kang, M. M. Ali, K. Zhang, E. J. Pone, and W. Zhao, TrAC Trends Anal. Chem. **58**, 145 (2014).
2. X. Pan, Single Cell Biol. **3**, 106 (2014).
3. F. S. O. Fritzsch, C. Dusny, O. Frick, and A. Schmid, Annu. Rev. Chem. Biomol. Eng. **3**, 129 (2012).
4. V. Backman, Y. Liu, P. Pradhan, Y. L. Kim, X. Li, A. Taflove, H. K. Roy, and R. Brand, *Frontiers in Optics, OSA Technical Digest (CD)* (Optical Society of America, 2006), paper FTuQ2.
5. H. Li, B. K. Smith, B. Shrestha, L. Márk, and A. Vertes, in *Mass Spectrometry Imaging of Small Molecules*, L. He, ed. (Humana, 2015), pp. 117–127.
6. M. K. Passarelli, C. F. Newman, P. S. Marshall, A. West, I. S. Gilmore, J. Bunch, M. R. Alexander, and C. T. Dollery, Anal. Chem. **87**, 6696 (2015).
7. H.-H. Cui and K.-M. Lim, Langmuir **25**, 3336 (2009).
8. D. Mondal, C. RoyChaudhuri, L. Das, and J. Chatterjee, Biomed. Microdevices **14**, 955 (2012).
9. B. Xu, S. Ji, D. Pan, W. Hu, S. Zhu, Y. Hu, J. Li, D. Wu, J. Chu, and K. Sugioka, Opt. Lett. **45**, 1071 (2020).
10. D. Di Carlo, L. Y. Wu, and L. P. Lee, Lab Chip **6**, 1445 (2006).
11. E. K. Sackmann, A. L. Fulton, and D. J. Beebe, Nature **507**, 181 (2014).
12. G. M. Whitesides, Nature **442**, 368 (2006).
13. X. Ding, S.-C. S. Lin, B. Kiraly, H. Yue, S. Li, I.-K. Chiang, J. Shi, S. J. Benkovic, and T. J. Huang, Proc. Natl. Acad. Sci. USA **109**, 11105 (2012).
14. J. R. Rettig and A. Folch, Anal. Chem. **77**, 5628 (2005).
15. K.-W. Huang, Y.-C. Wu, J.-A. Lee, and P.-Y. Chiou, Lab Chip **13**, 3721 (2013).
16. J. Kim, J. Erath, A. Rodriguez, and C. Yang, Lab Chip **14**, 2480 (2014).
17. L. Lin, Y.-S. Chu, J. P. Thiery, C. T. Lim, and I. Rodriguez, Lab Chip **13**, 714 (2013).
18. B. Xu, Y. Shi, Z. Lao, J. Ni, G. Li, Y. Hu, J. Li, J. Chu, D. Wu, and K. Sugioka, Lab Chip **18**, 442 (2018).
19. J. Yu, C. Zhou, W. Jia, W. Cao, S. Wang, J. Ma, and H. Cao, Appl. Opt. **51**, 1619 (2012).
20. L. Zhou, G.-L. Bai, X. Guo, S. Shen, Q.-D. Ou, and Y.-Y. Fan, Appl. Phys. Lett. **112**, 201902 (2018).
21. B. Xu, W.-Q. Du, J. Li, Y. Hu, L. Yang, C.-C. Zhang, G.-Q. Li, Z.-X. Lao, J.-C. Ni, J.-R. Chu, D. Wu, S.-L. Liu, and K. Sugioka, Sci. Rep. **6**, 19989 (2016).
22. Z.-Y. Zhang, C.-C. Zhang, Y.-L. Hu, C.-W. Wang, J.-W. Li, Y.-H. Su, J.-R. Chu, and D. Wu, Appl. Phys. Lett. **109**, 021109 (2016).
23. Y. Hu, Z. Wang, X. Wang, S. Ji, C. Zhang, J. Li, W. Zhu, D. Wu, and J. Chu, Light Sci. Appl. **9**, 119 (2020).